Published in final edited form as:

Hepatology. 2018 December ; 68(6): 2167–2181. doi:10.1002/hep.30060.

Preemptive activation of the integrated stress response protects mice from diet-induced obesity and insulin resistance via fibroblast growth factor 21 induction

Xu Xu[1,2], **Christopher Krumm**[1,2], **Jae-Seon So**[1,3], **Curtis J. Bare**[2,#], **Corey Holman**[2,#], **Jesper Gromada**[4], **David E. Cohen**[2], and **Ann-Hwee Lee**[1,4,*]

[1]Department of Pathology and Laboratory Medicine, Weill Cornell Medicine, New York, NY 10065

[2]Division of Gastroenterology and Hepatology, Joan & Sanford I. Weill Department of Medicine, Weill Cornell Medicine, New York, NY 10021, USA

[3]Department of Medical Biotechnology, Dongguk University Gyeongju, Gyeongju-si, Korea

[4]Regeneron Pharmaceuticals, Tarrytown, New York 10591, USA

Abstract

The integrated stress response (ISR) is a signaling system in which the phosphorylation of eukaryotic translation initiation factor 2α (eIF2α) by stress-specific kinases and the subsequent activation of activation transcription factor (ATF) 4 help restore cellular homeostasis following exposure to environmental stresses. ISR activation has been observed in metabolic diseases including hepatic steatosis, steatohepatitis and insulin resistance, but it remains unclear whether ISR contributes to the disease pathogenesis, or represents an innate defense mechanism against metabolic stresses. Constitutive repressor of eIF2α phosphorylation (CReP) is a critical regulatory subunit of the eIF2α phosphatase complex. Here we show that CReP ablation causes constitutive eIF2α phosphorylation in the liver, which leads to activation of the ATF4 transcriptional program including increased Fibroblast growth factor 21 (FGF21) production. Liver-specific CReP knockout ($CReP^{LKO}$) mice exhibited marked browning of white adipose tissue, increased energy expenditure and insulin sensitivity in a FGF21-dependent manner. Furthermore, $CReP^{LKO}$ mice were protected from high fat diet (HFD)-induced obesity, hepatic steatosis, and insulin resistance. Acute CReP ablation in the liver of HFD-induced obese mice also reduced adiposity and improved glucose homeostasis.

Conclusion—These data suggest that CReP abundance is a critical determinant for eIF2α phosphorylation and ensuing ISR activation in the liver. Constitutive ISR activation in the liver induces FGF21 and confers protection from high-fat diet (HFD)-induced adiposity, insulin resistance and hepatic steatosis in mice. Augmenting hepatic ISR may represent a novel therapeutic approach to treat metabolic disorders.

*Correspondence to: Ann-Hwee Lee, PhD, Regeneron Pharmaceuticals, 777 Old Saw Mill River Road, Tarrytown, NY 10591, Phone: 914-847-1997, annhwee.lee@regeneron.com.

#Equal contributions

INTRODUCTION

As a central component of the integrated stress response (ISR), eukaryotic translation initiation factor 2 (eIF2α) conveys diverse stress signals to decrease protein synthesis, while activating transcriptional program designed to cope with the stresses (1). Mammals have four kinases, general control nonrepressed 2 (GCN2), RNA-dependent protein kinase (PKR), PKR-like ER kinase (PERK), and heme-regulated eIF2α kinase (HRI) that are specifically activated by distinct stress signals, and commonly phosphorylate eIF2α at the Ser-51 residue (1). eIF2α phosphorylation decreases the efficiency of translational initiation, but paradoxically increases the translation of certain mRNAs that possess short open reading frames in the 5′ untranslated regions. It is well known that mRNAs encoding activation transcription factor (ATF) 4 and ATF5 are more efficiently translated as eIF2α phosphorylation is increased. ATF4 is considered a master transcriptional regulator of ISR and induces a variety of genes such as those involved in amino acid biosynthesis and redox regulation (2).

eIF2α phosphorylation is also regulated by phosphatase complexes which are composed of the catalytic subunit of protein phosphatase 1 (PP1) and regulatory subunits, growth arrest and DNA damage-inducible protein 34 (GADD34, encoded by *PPP1R15A*) or constitutive repressor of eIF2α phosphorylation (CReP, encoded by *PPP1R15B*) (3). Growth arrest and DNA damage-inducible protein 34 (GADD34) is induced by endoplasmic reticulum (ER) stress in a PERK-dependent manner, constituting a negative feedback loop regulating eIF2α phosphorylation (4). CReP was initially identified as a constitutively expressed PP1 activator that determines the basal level of eIF2α phosphorylation (3). However, recent study demonstrates that CReP abundance is dynamically regulated at the transcriptional, post-transcriptional and post-translational levels, and the abundance of CReP protein is a critical determinant of eIF2α phosphorylation (5–7). Independent of PP1 regulation, CReP can localize to membrane of intracellular vesicles and regulate membrane traffic (8).

Increased eIF2α phosphorylation has been observed in livers with steatosis, nonalcoholic and alcoholic hepatitis (9–14), but the physiological functions of ISR activation in these diseases remain unclear. Several studies suggested that ISR activation contribute to pathogenesis of liver steatosis. ATF4 has been shown to activate lipogenesis in hepatocytes (15–17), and increase the expression of hepatic very low-density lipoprotein receptor which contribute to the worsened hepatic steatosis (18). In line with this, ISR inhibition by the transgenic overexpression of GADD34 in the liver suppressed lipogenesis and protected the mice from hepatic steatosis (19). On the other hand, ISR has recently been identified as a potent inducer of a pleiotropic metabolic hormone, fibroblast growth factor 21 (FGF21) in response to various stresses (20–23). Notably, it has been shown that GCN2- or HRI-mediated FGF21 induction improves hepatic steatosis and glucose intolerance in mice (24, 25).

In the present study, we aim to determine whether ISR activation represents a part of a pathogenic mechanism in diseased organs, or an innate defense mechanism against metabolic stresses. We generated mutant mice lacking CReP selectively in hepatocytes, and demonstrated that the CReP ablation activated ISR independent of stresses. Surprisingly, we

found that the constitutive ISR activation caused a profound browning of white adipose tissues (WATs), increased whole body energy expenditure and insulin sensitivity, which leads to the protection from high-fat diet (HFD)-induced adiposity, insulin resistance and hepatic steatosis in mice. We further demonstrated that the endocrine fibroblast growth factor FGF21 plays a critical role in the metabolic benefits conferred by the ISR activation. Our data suggest that augmenting ISR could be a novel therapeutic approach to treat metabolic diseases.

MATERIALS AND METHODS

Generation of mice lacking CReP in the liver (CReP^{LKO})

A 7.7 kb mouse genomic DNA fragment containing *Pppa1r15b* gene was retrieved from a BAC clone (RP23-304O9, Roswell Park Cancer Institute) by recombineering (26). A targeting vector containing two loxP sites, one in the first intron and the other one 222 bp downstream of CReP coding region, and a FRT-NEO-FRT cassette was generated as described elsewhere (27). Mouse embryonic stem cells were transfected with the targeting vector to obtain a recombined clone. Targeted ES cells were injected into C57BL/6 blastocysts to produce Ppp1r15b^{loxP};FRT-NEO-FRT mice. FRT-NEO-FRT cassette was removed by mating to Flp recombinase transgenic mice. Ppp1r15b^{loxP} mice were backcrossed for more than five generations onto C57BL/6 background, and crossed to Albumin-cre (B6.Cg-Tg(Alb-cre)21Mgn/J, Jackson Laboratory) mice to generate liver specific CReP knockout (CReP^{LKO}) mice. To generate liver specific CReP and Fgf21 double knock out mice (DKO), CReP^{LKO} mice were crossed with Fgf21^{loxp} (B6.129S6(SJL)-Fgf21tm1.2Djm/J, Jackson Laboratory) mice.

Diets and animal experiments

Mice were fed either standard chow diet containing 13.2% fat, 24.6% protein and 62.1% carbohydrate (kcal/100 kcal) (#5053, LabDiet) or a high fat diet containing 60% fat, 20% protein and 20% carbohydrate (#D12492, Research Diets). Mice were housed in a 12-hr light/dark cycle with *ad libitum* access to food and water. For GTT, mice were fasted overnight for 16 hours with free access to water and injected intraperitoneally (i.p.) with 4.5g/kg glucose. For ITT, mice were fasted 4 hours before i.p. injected with human insulin (0.75 U/kg; Eli Lilly, Indianapolis, IN). For tunicamycin injection, a dose of 2 mg/kg tunicamycin in 150mM Dextrose were i.p. injected and mice were sacrificed after 6 hours for further analysis. Male mice around two months old with body weight of 24±1 gram were used unless otherwise indicated. All animal experiments were approved by the Weill Cornell Medical College Institutional Animal Care and Use Committee.

Serum and liver metabolites measurement

Mice were euthanized by CO_2 following the recommended procedure of the American Veterinary Medical Association (AVMA Euthanasia Panel Report). Plasma was obtained from blood samples collected with Microvette CB 300LH (SARSTEDT, Nümbrecht, Germany). Tissues were resected, snap-frozen, and stored at −80°C until further analysis. Plasma triglyceride, NEFA, ketone bodies, ALT, insulin, FGF21, albumin and haptoglobin concentrations were determined using commercial assay kits (Serum Triglyceride

Determination Kit, Sigma; NEFA-HR (2), Wako Chemicals; Autokit Total Ketone Bodies, Wako Chemicals; Ultra-Sensitive Mouse Insulin ELISA Kit, Crystal Chem; Mouse/Rat FGF-21 Quantikine ELISA Kit, R&D Systems; Mouse albumin and haptoglobin ELISA kit, Abcam). Plasma Albumin and Haptoglobin levels Lipids were extracted from liver tissues with chloroform/methanol mixture (2:1 v/v) and quantitated using Serum Triglyceride Determination Kit (Sigma), as described previously (28). All assays were performed according to the manufacturer's instructions. Blood glucose levels were measured using Ascensia Breeze 2 Blood Glucose Monitoring System (Bayer).

Western blot analysis

Whole tissue lysate for adipose tissues and the liver was prepared by homogenization in RIPA buffer. Liver nuclear extracts were prepared, as described previously (29). For western blot analysis, the following primary antibodies were used: CReP (Proteintech, 14634), Phospho-eIF2α (Cell Signaling, 9721), eIF2α (Santa Cruz, sc-133132), PERK (Cell Signaling, 3192), GCN2 (Cell Signaling, 3302), ATF4/CREB-2 (Santa Cruz, sc-200), ATF5 (Proteintech, 15260), Lamin B1 (Santa Cruz, sc-56145), UCP1 (Abcam, ab10983), PPARα (Santa Cruz, sc-9000), Perilipin (Cell Signaling, 9349), Phospho-AKT (Cell Signaling, 9208), AKT (Cell Signaling, 9272). Antibodies for CREBH, ApoB, ApoE, IRE1α, XBP1s, and ATF6α were described previously (29, 30). Phos-tag western blot was performed as previously described (29).

Statistical analysis

All data are expressed as mean ± SEM for experiments including numbers of mice or duplicates as indicated. The two-tailed Student's test was used to evaluate statistical differences between groups. Two-way ANOVA with replication was performed to analyze data obtained with time-course experiments. Statistics of significance was expressed as the number of asterisks: * = $p< 0.05$; ** = $p< 0.01$; *** = $p< 0.001$.

RESULTS

CReP ablation increases eIF2α phosphorylation and activates ATF4-dependent transcription program in the liver

To determine the role of CReP in eIF2α phosphorylation in the liver, we generated liver-specific CReP knockout ($CReP^{LKO}$) mice by crossing $Ppp1r15b^{loxP}$ mice with Albumin-Cre mice expressing Cre recombinase under the control of mouse albumin enhancer/promoter. *Ppp1r15b* gene contains two exons, and Cre recombinase-mediated deletion of exon 2 is expected to produce C-terminal truncated CReP protein devoid of PP1 and eIF2α binding domains (Figure S1A) (31). Contrary to the full length CReP, overexpression in HeLa cells of the mutant CReP lacking exon 2 sequences failed to suppress UV-mediated eIF2α phosphorylation, confirming that the mutant protein is incapable of promoting eIF2α de-phosphorylation (Figure S1B). Both WT and the mutant CReP were rapidly degraded by UV-irradiation (Figure S1B), consistent with a previous report (5). Efficient CReP ablation in $CReP^{LKO}$ liver was confirmed by western blotting and quantitative RT-PCR analyses (Figure 1A and S1C). $CReP^{LKO}$ mice were born at a normal Mendelian ratio, and appeared grossly normal. Interestingly, liver to body weight ratio was reduced by 14% in $CReP^{LKO}$

mice (Figure S1D). Liver damage was not observed in CReP^{LKO} mice, as determined by histological analysis of liver sections and ALT assay (Figure 1B and 1C). Plasma protein concentrations and the levels of major liver-secreted proteins such as albumin, haptoglobin, and apolipoproteins B and E were comparable between WT and CReP^{LKO} mice (Figure 1D and S2A-E). These data suggested that CReP deletion had minimal effect on protein synthetic and secretory function of the liver.

eIF2α phosphorylation was markedly increased in CReP^{LKO} livers (Figure 1A and S1E), suggesting that CReP expression is critical for eIF2α dephosphorylation in hepatocytes. Consistent with the induction of eIF2α phosphorylation, ATF4 and ATF5 proteins were markedly induced in CReP^{LKO} livers (Figure 1A). mRNA levels of ATF4-dependent genes such as *Atf5*, *Asns*, and *Psat1* were also increased in CReP^{LKO} livers (Figure 1E). FGF21, a liver-derived hormone exerting various metabolic benefits, was highly expressed in CReP^{LKO} livers, consistent with previous studies demonstrating the role of ATF4 in FGF21 expression (20–22). Notably, certain ATF4-dependent ER stress-inducible genes such as *Hspa5, Ddit3*, and *Ppp1r15a* were not induced or only minimally induced in CReP^{LKO} livers (Figure 1E), indicating that the ISR activation by CReP deletion is qualitatively different from stress-mediated UPR. On the other hand, other ER stress markers such as phospho-PERK, phospho-IRE1α, spliced X-box-binding protein 1 (XBP1s), the nuclear ATF6α proteins were not increased in CReP^{LKO} livers (Figure 1A, 1B, and S3A), excluding the possibility of increased ER stress inducing eIF2α phosphorylation. In fact, basal XBP1s protein level was modestly reduced in CReP^{LKO} livers, likely reflecting reduced basal stress level (Figure 1A). Representative UPR markers were comparably expressed between WT and CReP^{LKO} mice in both basal and HFD-fed conditions (Figure S3C-D). Tunicamycin, an ER stress-inducing agent, strongly activated ER stress markers (Figure 1A) and induced ER stress responsive genes in both WT and CReP^{LKO} livers (Figure 1E). Interestingly, CReP^{LKO} mice exhibited modestly reduced expression of a subset of ER stress response genes, such as *Dnajb9*, *Dnajc3*, *Edem1, Ero1l, Hsp90b1*, and *Pdia3* compared with WT mice upon tunicamycin treatment (Figure S3A), suggesting that the ISR activation by CReP deletion may dampen ER stress response. Tunicamycin-mediated liver damage determined by alanine aminotransferase (ALT) assay was comparable between WT and CReP^{LKO} mice (Figure S3E). GCN2 phosphorylation was also unaffected in the liver of CReP^{LKO} mice (Figure 1A). These data indicate that CReP ablation increased eIF2α phosphorylation and turned on ISR signaling without inducing stress *per se*.

ATF4-dependent FGF21 expression in CReP^{LKO} mice promotes beige adipogenesis and improved glucose homeostasis

In mice, hepatic FGF21 is strongly induced by fasting (28, 32, 33). Fed-state hepatic FGF21 mRNA and plasma FGF21 protein levels in CReP^{LKO} mice were comparable to those of fasted WT mice (Figure 2A and 2B). Fasting further increased FGF21 expression in CReP^{LKO} mice (Figure 2A).

Hepatic FGF21 expression is controlled by several transcription factors such as ATF4, cyclic-AMP-responsive-element-binding protein H (CREBH) and peroxisome proliferator-activated receptor α (PPARα) (20, 28, 32–34). While ATF4 mediates FGF21 expression

during ER stress and amino acid insufficiency (20, 24), CREBH and PPARα are critical for fasting- and ketogenic diet-mediated FGF21 expression (28, 32, 34). Hepatic CREBH and PPARα mRNA and protein expression was largely unaffected by CReP deletion (Figure 2B and S2). Representative CREBH- and PPARα- dependent genes were strongly induced by fasting similarly in both WT and CReP^{LKO} livers (Figure S4), indicating that CReP deletion had minimal effects on CREBH and PPARα expression and function, and that FGF21 induction in CReP^{LKO} livers is independent of CREBH or PPARα. On the other hand, siRNA-mediated silencing of ATF4 drastically reduced hepatic FGF21 expression and plasma FGF21 levels in CReP^{LKO} mice, along with other ATF4 target genes such as *Asns* and *Psat1* (Figure 2C and 2D), suggesting that ATF4 plays a critical role in FGF21 induction in CReP^{LKO} liver. Interestingly, transfection of various combinations of transcription factors into HepG2 cells suggests that ATF4 is the most potent inducer of FGF21 expression, while CREBH and PPARα further augment ATF4-dependent FGF21 expression (Figure 2E).

Given the robust FGF21 production in CReP^{LKO} mice, we next asked whether these mice exhibited metabolic phenotypes reflecting the beneficial effects of FGF21. CReP^{LKO} mice contained strikingly brown-colored subcutaneous inguinal white adipose tissue (iWAT) (Figure 3A), suggesting the browning of WAT. Indeed, H&E staining revealed abundant multilocular brown adipocyte-like cells in the iWAT of CReP^{LKO}, but not in WT mice (Fig 3A). Brown adipocyte markers such as uncoupling protein 1 (*Ucp1*), deiodinase type 2 (*Dio2*), and ELOVL fatty acid elongase 3 (*Elovl3*) were also highly induced in the iWAT of CReP^{LKO} mice (Figure 3B and S5A), suggesting the occurrence of browning of WAT in these mice. Western blotting analysis showed marked induction of UCP1 protein in iWAT of CReP^{LKO} mice (Figure 3C). UCP1 and Eovl3 mRNA levels were also increased in BAT of CReP^{LKO} mice by 1.8- and 4-fold, respectively compared with the WT controls (Fig 3B and S5B), which correlated well with denser eosinophilic staining of BAT sections of the former (Figure 3A). CReP deletion also increased UCP1 mRNA level in epididymal WAT (eWAT) of CReP^{LKO} mice (Figure 3B). We next measured energy expenditure parameters in CReP^{LKO} mice by indirect calorimetry. Compared with WT, CReP^{LKO} mice exhibited markedly increased energy expenditure (EE), rates of O_2 consumption (VO_2), and CO_2 production (VCO_2) (Figure 3D). Importantly, respiratory exchange ratio (RER) was significantly lower in CReP^{LKO} mice, indicating a higher consumption of fat as energy source, consistent with the fat browning phenotype in these mice (Figure 3D). No difference was observed in food intake per animal and physical activity between WT and CReP^{LKO} mice, while water intake per animal appeared higher in CReP^{LKO} mice during the dark phase (Figure S5C). When normalized to body weight, CReP^{LKO} mice exhibited higher intake of both food and water during the dark phase (Figure S5D). To test whether systemic insulin sensitivity was increased in CReP^{LKO} mice, we performed glucose tolerance test (GTT) and insulin tolerance test (ITT). Both GTT and ITT showed substantially improved insulin sensitivity and glucose homeostasis in CReP^{LKO} mice (Figure 3E and 3F). Insulin-mediated AKT phosphorylation in the liver and WAT was also higher in CReP^{LKO} mice compared with WT controls (Figure S5E). Taken together, these data indicate that CReP deletion in the liver increases the production of FGF21, promotes the browning of WAT, and increases whole body energy expenditure and insulin sensitivity.

CReP^{LKO} mice are resistant to high fat diet-induced metabolic abnormalities

We next evaluated the impact of CReP deletion on high fat diet (HFD)-induced metabolic abnormalities including obesity, insulin resistance, and hepatic steatosis. The body weight of CReP^{LKO} mice prior to start of HFD feeding was 17% lower compared with the littermate controls (Figure 4A). After 10 weeks of HFD feeding, the difference in BW was more pronounced with CReP^{LKO} mice weighing 32% less compared with the controls (Figure 4A). Importantly, the percentage of fat mass in CReP^{LKO} mice was significantly reduced with a concomitant increase in lean mass percentage compared with the WT controls, indicating the marked reduction in adiposity in CReP^{LKO} mice (Figure 4A).

HFD feeding increased blood glucose and serum insulin levels in WT mice (Figure 4B), reflecting the onset of insulin resistance. In contrast, CReP^{LKO} mice maintained normal blood glucose and serum insulin levels during the course of HFD feeding (Figure 4B). Consistently, CReP^{LKO} mice exhibited improved glucose homeostasis, as determined by GTT and ITT (Figure 4C).

CReP^{LKO} mice maintained high serum FGF21 levels throughout HFD feeding, whereas HFD feeding only modestly increased serum FGF21 levels in WT mice (Figure 4B). This is likely due to the development of hepatic steatosis in these mice, which is known to induce FGF21 through PPARα and CREBH (28). Indeed, HFD feeding induced hepatic steatosis in WT mice, as demonstrated by the presence of abundant lipid droplets in the liver sections (Figure 4D), and biochemical quantification of hepatic TG content (Figure 4E). HFD-induced hepatic steatosis was markedly improved in CReP^{LKO} mice (Figure 4D and 4E). We found that the proteolytic activation of a key lipogenic transcription factor, SREBP-1c (Figure 4E), and the expression of its target lipogenic genes were down-regulated in CReP^{LKO} livers (Figure 4E).

We next examined whether increased whole-body energy expenditure might have contributed to the decreased adiposity, and the improved glucose and lipid homeostasis in CReP^{LKO} mice. Indirect calorimetry revealed that the VO_2, VCO_2, and energy expenditure were markedly increased in CReP^{LKO} mice (Figure 4F). Browning of WAT as demonstrated by the increased abundance of adipocytes containing multilocular lipid droplets (Figure 4D), and the induction of Ucp1, Elvol3 and other thermogenic genes in iWAT and BAT was observed in HFD-fed CReP^{LKO} mice (Figure S6A and S6B), consistent with the observation in chow-fed mice. Plasma ketones tended to be elevated in CReP^{LKO} mice, suggesting increased ketogenesis (Figure S6C). Plasma non-esterified fatty acid (NEFA) and TG levels were reduced in CReP^{LKO} mice (Figure S6D and S6E). These data suggest that ISR activation in CReP^{LKO} mice increases the production of FGF21, which in turn increases whole-body energy expenditure, and confers protection of CReP^{LKO} mice from diet-induced obesity and the associated metabolic disorders.

Effects of acute CReP deletion in the liver

The profound improvement of metabolic parameters in CReP^{LKO} mice suggests that ISR activation in the liver would be a potential therapeutic strategy to treat metabolic disorders. To investigate the effects of ISR activation in adult mice, we used recombinant adeno-

associated virus (AAV) expressing Cre recombinase under the control of the liver-specific thyroxine-binding globulin promoter (AAV-cre). Injection of AAV-cre into Ppp1r15b^{loxP} mice led to almost complete ablation of CReP mRNA expression (Figure S7A). As anticipated, *Fgf21*, *Asns*, and *Psat1* were highly expressed in the liver of the AAV-cre-injected Ppp1r15b^{loxP} mice (Figure S7A). Consistent with what we observed in CReP^{LKO} mice, certain ER stress-inducible ATF4 target genes such as *Ddit3*, and *Ppp1r15a* were not induced by acute CReP deletion (Figure S7B). Nuclear XBP1s and phospho-PERK levels tended to be decreased in CReP deleted livers (Figure S7C). Acute CReP deletion did not cause liver damage (Figure S7D). *Ucp1* and *Elov3* expression in iWAT and BAT were increased by AAV-cre injection (Figure 5A), which correlated well with the appearance of adipocytes with small lipid droplets (Figure 5B). AAV-cre injection into Ppp1r15b^{loxP} mice resulted in 6% reduction in body weight and 20% reduction in blood glucose level within 3 days, which were maintained up to more than 4 weeks (Figure 5C and data not shown).

To further test the beneficial metabolic effects of CReP ablation in diet induced obese (DIO) mice, we injected AAV-cre into HFD-fed Ppp1r15b^{loxP} mice. Body weight and blood glucose level gradually decreased over 2 weeks by 20% and 45%, respectively, in HFD-fed Ppp1r15b^{loxP} mice injected with AAV-cre (Figure 5C). Remarkably, CReP ablation decreased fat mass, resulting in an increase of the lean mass ratio in these mice (Figure 5D). ITT further revealed a dramatic improvement of insulin sensitivity by the acute CReP deletion in DIO mice (Figure 5E). Liver steatosis induced by HFD was also improved by AAV-cre injection (Figure 5F and Figure S7E). Collectively, these data demonstrate that augmenting ISR in the liver by CReP ablation has multiple beneficial metabolic effects on obesity and type 2 diabetes.

FGF21 is critical for metabolic benefit in CReP^{LKO} mice

To investigate the importance of FGF21 in the improved metabolic parameters of CReP^{LKO} mice, we generated liver-specific CReP and FGF21 double knockout (DKO) mice by crossing CReP^{LKO} with Fgf21^{loxP} mice. Loss of CReP and FGF21 mRNA expression in DKO liver was confirmed by qPCR (Figure S8A). Induction of Ucp1 and Elovl3 mRNAs in CReP^{LKO} mice were completely reversed by the concomitant loss of FGF21 in DKO mice (Figure 6A and 6B). As anticipated, browning of iWAT in CReP^{LKO} mice was also reversed in DKO mice (Figure 6C). Increased energy expenditure (EE), rates of O_2 consumption (VO_2), and CO_2 production (VCO_2) and decreased RER in CReP^{LKO} mice were normalized in DKO mice (Figure 6E). DKO mice had significantly higher body weight than CReP^{LKO}, suggesting that the elevated FGF21 level is responsible for the delayed weight gain of CReP^{LKO} mice (Figure 6D). The improved insulin sensitivity and glucose homeostasis of CReP^{LKO} mice was also abolished by the concomitant FGF21 ablation in DKO mice as indicated by ITT and GTT (Figure 6F and S8B). These data suggest that FGF21 is a critical ISR-regulated gene that confers metabolic benefits in CReP^{LKO} mice.

DISCUSSION

ISR has been appreciated as a cytoprotective mechanism against environmental stresses. Diminished protein synthesis by eIF2α phosphorylation is believed to conserve amino acids

and energy, which could be used for the expression of ATF4-dependent cytoprotective genes (2). Consistently, genetic ablation of eIF2α kinases or ATF4, or mutation at the phosphorylation site of eIF2α causes various impairments in development, cell survival, and organ functions (35). It is conceivable that augmenting ISR has beneficial effects on cell survival and function. Particularly in the liver, it has been shown that ISR activation results in a dramatic induction of FGF21 (23–25), implying a potential metabolic function of ISR. In this study, we explored the role of CReP in ISR activation in the liver, and the impact of ISR activation via CReP ablation on liver function. We found that CReP ablation caused constitutive eIF2α phosphorylation and activation of ATF4-dependent ISR target gene expression in the liver. ATF4-dependent FGF21 expression by CReP deletion conferred multiple metabolic benefits in HFD-induced obese mice including weight loss, improved glycemic control, and protection from hepatic steatosis. This study reveals that ISR activation in the liver is beneficial to systemic metabolic health. Strategies to target CReP or disrupt CReP-PP1 interaction could be promising methods to boost ISR. Phosphatase inhibitors could also be used to target ISR for the same purpose. For example, Salubrinal has been reported to inhibit phosphatase activation and therefore activate ISR pathway (36). It is necessary to investigate whether these methods could be applied to the treatment of metabolic diseases.

FGF21 is a hepatokine that has multiple metabolic activities including improvement of obesity, hyperglycemia, dyslipidemia, and hepatic steatosis (37–39). Accordingly, FGF21 signaling has received significant attention as a therapeutic target for anti-obesity and anti-diabetes drugs (40, 41). Various approaches have been employed to develop FGF21-based therapeutic molecules, including long-acting FGF21 analogs and agonist antibodies for FGF21 receptor complex (40, 41). Targeting ISR represents a novel strategy to increase endogenous FGF21 expression. It is notable that plasma FGF21 level in $CReP^{LKO}$ mice is comparable to fasting-induced FGF21 level in WT mice, which might be beneficial in minimizing potential side effects of using supraphysiological doses of FGF21-mimetics.

Increased eIF2α phosphorylation by CReP deletion presumes that certain eIF2α kinases are basally active in normal mouse liver to provide phosphorylated eIF2α that would accumulate when its dephosphorylation is inhibited. Indeed, we were able to detect basal eIF2α phosphorylation in normal mouse liver, which was further enhanced in the absence of CReP. Similarly, silencing of CReP in cultured cells strongly increased eIF2α phosphorylation, suggesting the presence of basal eIF2α kinase activity in these cells (5–7). We hypothesize that low-grade stress signals may be present in most cells under normal physiological condition. The identity of basal stress and the kinase responsible for the basal eIF2α phosphorylation in various settings remain to be determined.

ATF4 is considered a master transcriptional regulator of the ISR, regulating a variety of genes including those involved in amino acid biosynthesis and transport, redox regulation, and feedback regulation of ISR (2, 42). ATF4 is also a potent FGF21 inducer (20, 21). Knockdown of ATF4 expression by siRNA decreased FGF21 production in CReP deficient liver, identifying ATF4 as a critical FGF21 inducer. CReP ablation in the liver-specific FGF21 knockout mice failed to lower body weight and increase insulin sensitivity, indicating that FGF21 is the critical factor downstream of CReP/eIF2α/ATF4 pathway

responsible for the improved metabolic parameters in CReP^{LKO} mice. In summary, we propose that CReP deletion activates a linear signaling pathway involving eIF2α phosphorylation, ATF4 translation and FGF21 induction, which promotes increased energy expenditure, and subsequently improved obesity-related metabolic parameters (Figure 7). It is notable, however, that ISR affects many other genes at translational and transcriptional levels which might also participate to metabolic regulation. For example, ATF5 is also highly induced in CReP knockout liver. Similar to ATF4, ATF5 mRNA has two short ORFs in the 5′ UTR that allow preferential translation of ATF5 upon eIF2α phosphorylation (43, 44). ATF5 is highly expressed in the liver, and has emerged as an important regulator of mitochondrial respiration and cell proliferation (43, 45–47). Given the increased ketone production in CReP^{LKO} mice, ATF5 might stimulate fatty acid oxidation and oxidative phosphorylation in mitochondria, contributing to the increased energy expenditure and prevention of excessive TG accumulation in the liver. Future studies will define the role of ATF5 in CReP deficient liver.

Supplementary Material

Refer to Web version on PubMed Central for supplementary material.

Acknowledgments

This work was supported by US National Institutes of Health grants R01DK089211 (to A-.H.L.), and R37DK048873, R01DK056626 and R01DK103046 (to D.E.C.). X.X. is supported by American Heart Association postdoctoral fellowship (17POST32330002).

ABBREVIATIONS

AAV	adeno-associated virus
ALT	alanine aminotransferase
ATF	activation transcription factor
BAT	brown adipose tissue
CREBH	cyclic-AMP-responsive-element-binding protein H
CReP	constitutive repressor of eIF2α phosphorylation
DKO	double knockout
EE	energy expenditure
ER	endoplasmic reticulum
eWAT	epididymal WAT
Fgf21	fibroblast growth factor 21
GADD34	growth arrest and DNA damage-inducible protein 34
GCN2	general control nonrepressed 2

GTT	glucose tolerance test
HFD	high-fat diet
HRI	heme-regulated eIF2α kinase
ISR	integrated stress response
ITT	Insulin tolerance test
iWAT	inguinal white adipose tissue
PERK	PKR-like ER kinase
PKR	RNA-dependent protein kinase
PP1	protein phosphatase 1
PPARα	peroxisome proliferator-activated receptor α
RER	respiratory exchange ratio
VO_2	rate of O_2 consumption
VCO_2	rate of CO_2 production
WAT	white adipose tissue
XBP1	X-box-binding protein 1

References

1. Wek RC, Cavener DR. Translational control and the unfolded protein response. Antioxid Redox Signal. 2007; 9:2357–2371. [PubMed: 17760508]
2. Harding HP, Zhang Y, Zeng H, Novoa I, Lu PD, Calfon M, Sadri N, et al. An integrated stress response regulates amino acid metabolism and resistance to oxidative stress. Mol Cell. 2003; 11:619–633. [PubMed: 12667446]
3. Jousse C, Oyadomari S, Novoa I, Lu P, Zhang Y, Harding HP, Ron D. Inhibition of a constitutive translation initiation factor 2alpha phosphatase, CReP, promotes survival of stressed cells. J Cell Biol. 2003; 163:767–775. [PubMed: 14638860]
4. Novoa I, Zeng H, Harding HP, Ron D. Feedback inhibition of the unfolded protein response by GADD34-mediated dephosphorylation of eIF2alpha. J Cell Biol. 2001; 153:1011–1022. [PubMed: 11381086]
5. Loveless TB, Topacio BR, Vashisht AA, Galaang S, Ulrich KM, Young BD, Wohlschlegel JA, et al. DNA Damage Regulates Translation through beta-TRCP Targeting of CReP. PLoS Genet. 2015; 11:e1005292. [PubMed: 26091241]
6. De Gassart A, Bujisic B, Zaffalon L, Decosterd LA, Di Micco A, Frera G, Tallant R, et al. An inhibitor of HIV-1 protease modulates constitutive eIF2alpha dephosphorylation to trigger a specific integrated stress response. Proc Natl Acad Sci U S A. 2016; 113:E117–126. [PubMed: 26715744]
7. So JS, Cho S, Min SH, Kimball SR, Lee AH. IRE1alpha-Dependent Decay of CReP/Ppp1r15b mRNA Increases Eukaryotic Initiation Factor 2alpha Phosphorylation and Suppresses Protein Synthesis. Mol Cell Biol. 2015; 35:2761–2770. [PubMed: 26031337]
8. Kloft N, Neukirch C, von Hoven G, Bobkiewicz W, Weis S, Boller K, Husmann M. A subunit of eukaryotic translation initiation factor 2alpha-phosphatase (CreP/PPP1R15B) regulates membrane traffic. J Biol Chem. 2012; 287:35299–35317. [PubMed: 22915583]

9. Soon RK Jr, Yan JS, Grenert JP, Maher JJ. Stress signaling in the methionine-choline-deficient model of murine fatty liver disease. Gastroenterology. 2010; 139:1730–1739. 1739 e1731. [PubMed: 20682321]
10. Henkel AS, Dewey AM, Anderson KA, Olivares S, Green RM. Reducing endoplasmic reticulum stress does not improve steatohepatitis in mice fed a methionine- and choline-deficient diet. Am J Physiol Gastrointest Liver Physiol. 2012; 303:G54–59. [PubMed: 22556147]
11. Magne L, Blanc E, Legrand B, Lucas D, Barouki R, Rouach H, Garlatti M. ATF4 and the integrated stress response are induced by ethanol and cytochrome P450 2E1 in human hepatocytes. J Hepatol. 2011; 54:729–737. [PubMed: 21146245]
12. Wang D, Wei Y, Pagliassotti MJ. Saturated fatty acids promote endoplasmic reticulum stress and liver injury in rats with hepatic steatosis. Endocrinology. 2006; 147:943–951. [PubMed: 16269465]
13. Ozcan U, Cao Q, Yilmaz E, Lee AH, Iwakoshi NN, Ozdelen E, Tuncman G, et al. Endoplasmic reticulum stress links obesity, insulin action, and type 2 diabetes. Science. 2004; 306:457–461. [PubMed: 15486293]
14. Puri P, Mirshahi F, Cheung O, Natarajan R, Maher JW, Kellum JM, Sanyal AJ. Activation and dysregulation of the unfolded protein response in nonalcoholic fatty liver disease. Gastroenterology. 2008; 134:568–576. [PubMed: 18082745]
15. Li H, Meng Q, Xiao F, Chen S, Du Y, Yu J, Wang C, et al. ATF4 deficiency protects mice from high-carbohydrate-diet-induced liver steatosis. Biochem J. 2011; 438:283–289. [PubMed: 21644928]
16. Li K, Xiao Y, Yu J, Xia T, Liu B, Guo Y, Deng J, et al. Liver-specific Gene Inactivation of the Transcription Factor ATF4 Alleviates Alcoholic Liver Steatosis in Mice. J Biol Chem. 2016; 291:18536–18546. [PubMed: 27405764]
17. Xiao G, Zhang T, Yu S, Lee S, Calabuig-Navarro V, Yamauchi J, Ringquist S, et al. ATF4 protein deficiency protects against high fructose-induced hypertriglyceridemia in mice. J Biol Chem. 2013; 288:25350–25361. [PubMed: 23888053]
18. Jo H, Choe SS, Shin KC, Jang H, Lee JH, Seong JK, Back SH, et al. Endoplasmic reticulum stress induces hepatic steatosis via increased expression of the hepatic very low-density lipoprotein receptor. Hepatology. 2013; 57:1366–1377. [PubMed: 23152128]
19. Oyadomari S, Harding HP, Zhang Y, Oyadomari M, Ron D. Dephosphorylation of translation initiation factor 2alpha enhances glucose tolerance and attenuates hepatosteatosis in mice. Cell Metab. 2008; 7:520–532. [PubMed: 18522833]
20. De Sousa-Coelho AL, Marrero PF, Haro D. Activating transcription factor 4-dependent induction of FGF21 during amino acid deprivation. Biochem J. 2012; 443:165–171. [PubMed: 22233381]
21. Kim KH, Jeong YT, Oh H, Kim SH, Cho JM, Kim YN, Kim SS, et al. Autophagy deficiency leads to protection from obesity and insulin resistance by inducing Fgf21 as a mitokine. Nat Med. 2013; 19:83–92. [PubMed: 23202295]
22. Schaap FG, Kremer AE, Lamers WH, Jansen PL, Gaemers IC. Fibroblast growth factor 21 is induced by endoplasmic reticulum stress. Biochimie. 2013; 95:692–699. [PubMed: 23123503]
23. Fusakio ME, Willy JA, Wang Y, Mirek ET, Al Baghdadi RJ, Adams CM, Anthony TG, et al. Transcription factor ATF4 directs basal and stress-induced gene expression in the unfolded protein response and cholesterol metabolism in the liver. Mol Biol Cell. 2016; 27:1536–1551. [PubMed: 26960794]
24. Laeger T, Albarado DC, Burke SJ, Trosclair L, Hedgepeth JW, Berthoud HR, Gettys TW, et al. Metabolic Responses to Dietary Protein Restriction Require an Increase in FGF21 that Is Delayed by the Absence of GCN2. Cell Rep. 2016; 16:707–716. [PubMed: 27396336]
25. Zarei M, Barroso E, Leiva R, Barniol-Xicota M, Pujol E, Escolano C, Vazquez S, et al. Heme-Regulated eIF2alpha Kinase Modulates Hepatic FGF21 and Is Activated by PPARbeta/delta Deficiency. Diabetes. 2016; 65:3185–3199. [PubMed: 27486236]
26. Liu P, Jenkins NA, Copeland NG. A highly efficient recombineering-based method for generating conditional knockout mutations. Genome Res. 2003; 13:476–484. [PubMed: 12618378]

27. Bouvier J, Cheng JG. Recombineering-based procedure for creating Cre/loxP conditional knockouts in the mouse. Curr Protoc Mol Biol. 2009:13. Chapter 23: Unit 23. [PubMed: 19170029]
28. Park JG, Xu X, Cho S, Hur KY, Lee MS, Kersten S, Lee AH. CREBH-FGF21 axis improves hepatic steatosis by suppressing adipose tissue lipolysis. Sci Rep. 2016; 6:27938. [PubMed: 27301791]
29. Lee AH, Scapa EF, Cohen DE, Glimcher LH. Regulation of hepatic lipogenesis by the transcription factor XBP1. Science. 2008; 320:1492–1496. [PubMed: 18556558]
30. Lee JH, Giannikopoulos P, Duncan SA, Wang J, Johansen CT, Brown JD, Plutzky J, et al. The transcription factor cyclic AMP-responsive element-binding protein H regulates triglyceride metabolism. Nat Med. 2011; 17:812–815. [PubMed: 21666694]
31. Rojas M, Vasconcelos G, Dever TE. An eIF2alpha-binding motif in protein phosphatase 1 subunit GADD34 and its viral orthologs is required to promote dephosphorylation of eIF2alpha. Proc Natl Acad Sci U S A. 2015; 112:E3466–3475. [PubMed: 26100893]
32. Badman MK, Pissios P, Kennedy AR, Koukos G, Flier JS, Maratos-Flier E. Hepatic fibroblast growth factor 21 is regulated by PPARalpha and is a key mediator of hepatic lipid metabolism in ketotic states. Cell Metab. 2007; 5:426–437. [PubMed: 17550778]
33. Inagaki T, Dutchak P, Zhao G, Ding X, Gautron L, Parameswara V, Li Y, et al. Endocrine regulation of the fasting response by PPARalpha-mediated induction of fibroblast growth factor 21. Cell Metab. 2007; 5:415–425. [PubMed: 17550777]
34. Kim H, Mendez R, Zheng Z, Chang L, Cai J, Zhang R, Zhang K. Liver-enriched transcription factor CREBH interacts with peroxisome proliferator-activated receptor alpha to regulate metabolic hormone FGF21. Endocrinology. 2014; 155:769–782. [PubMed: 24424044]
35. Dara L, Ji C, Kaplowitz N. The contribution of endoplasmic reticulum stress to liver diseases. Hepatology. 2011; 53:1752–1763. [PubMed: 21384408]
36. Boyce M, Bryant KF, Jousse C, Long K, Harding HP, Scheuner D, Kaufman RJ, et al. A selective inhibitor of eIF2alpha dephosphorylation protects cells from ER stress. Science. 2005; 307:935–939. [PubMed: 15705855]
37. Kharitonenkov A, Shiyanova TL, Koester A, Ford AM, Micanovic R, Galbreath EJ, Sandusky GE, et al. FGF-21 as a novel metabolic regulator. J Clin Invest. 2005; 115:1627–1635. [PubMed: 15902306]
38. Coskun T, Bina HA, Schneider MA, Dunbar JD, Hu CC, Chen Y, Moller DE, et al. Fibroblast growth factor 21 corrects obesity in mice. Endocrinology. 2008; 149:6018–6027. [PubMed: 18687777]
39. Xu J, Lloyd DJ, Hale C, Stanislaus S, Chen M, Sivits G, Vonderfecht S, et al. Fibroblast growth factor 21 reverses hepatic steatosis, increases energy expenditure, and improves insulin sensitivity in diet-induced obese mice. Diabetes. 2009; 58:250–259. [PubMed: 18840786]
40. Sonoda J, Chen MZ, Baruch A. FGF21-receptor agonists: an emerging therapeutic class for obesity-related diseases. Horm Mol Biol Clin Investig. 2017; 30
41. Gimeno RE, Moller DE. FGF21-based pharmacotherapy–potential utility for metabolic disorders. Trends Endocrinol Metab. 2014; 25:303–311. [PubMed: 24709036]
42. Kilberg MS, Balasubramanian M, Fu L, Shan J. The transcription factor network associated with the amino acid response in mammalian cells. Adv Nutr. 2012; 3:295–306. [PubMed: 22585903]
43. Zhou D, Palam LR, Jiang L, Narasimhan J, Staschke KA, Wek RC. Phosphorylation of eIF2 directs ATF5 translational control in response to diverse stress conditions. J Biol Chem. 2008; 283:7064–7073. [PubMed: 18195013]
44. Watatani Y, Ichikawa K, Nakanishi N, Fujimoto M, Takeda H, Kimura N, Hirose H, et al. Stress-induced translation of ATF5 mRNA is regulated by the 5′-untranslated region. J Biol Chem. 2008; 283:2543–2553. [PubMed: 18055463]
45. Fiorese CJ, Schulz AM, Lin YF, Rosin N, Pellegrino MW, Haynes CM. The Transcription Factor ATF5 Mediates a Mammalian Mitochondrial UPR. Curr Biol. 2016; 26:2037–2043. [PubMed: 27426517]

46. Hansen MB, Mitchelmore C, Kjaerulff KM, Rasmussen TE, Pedersen KM, Jensen NA. Mouse Atf5: molecular cloning of two novel mRNAs, genomic organization, and odorant sensory neuron localization. Genomics. 2002; 80:344–350. [PubMed: 12213205]

47. Shimizu YI, Morita M, Ohmi A, Aoyagi S, Ebihara H, Tonaki D, Horino Y, et al. Fasting induced up-regulation of activating transcription factor 5 in mouse liver. Life Sci. 2009; 84:894–902. [PubMed: 19376136]

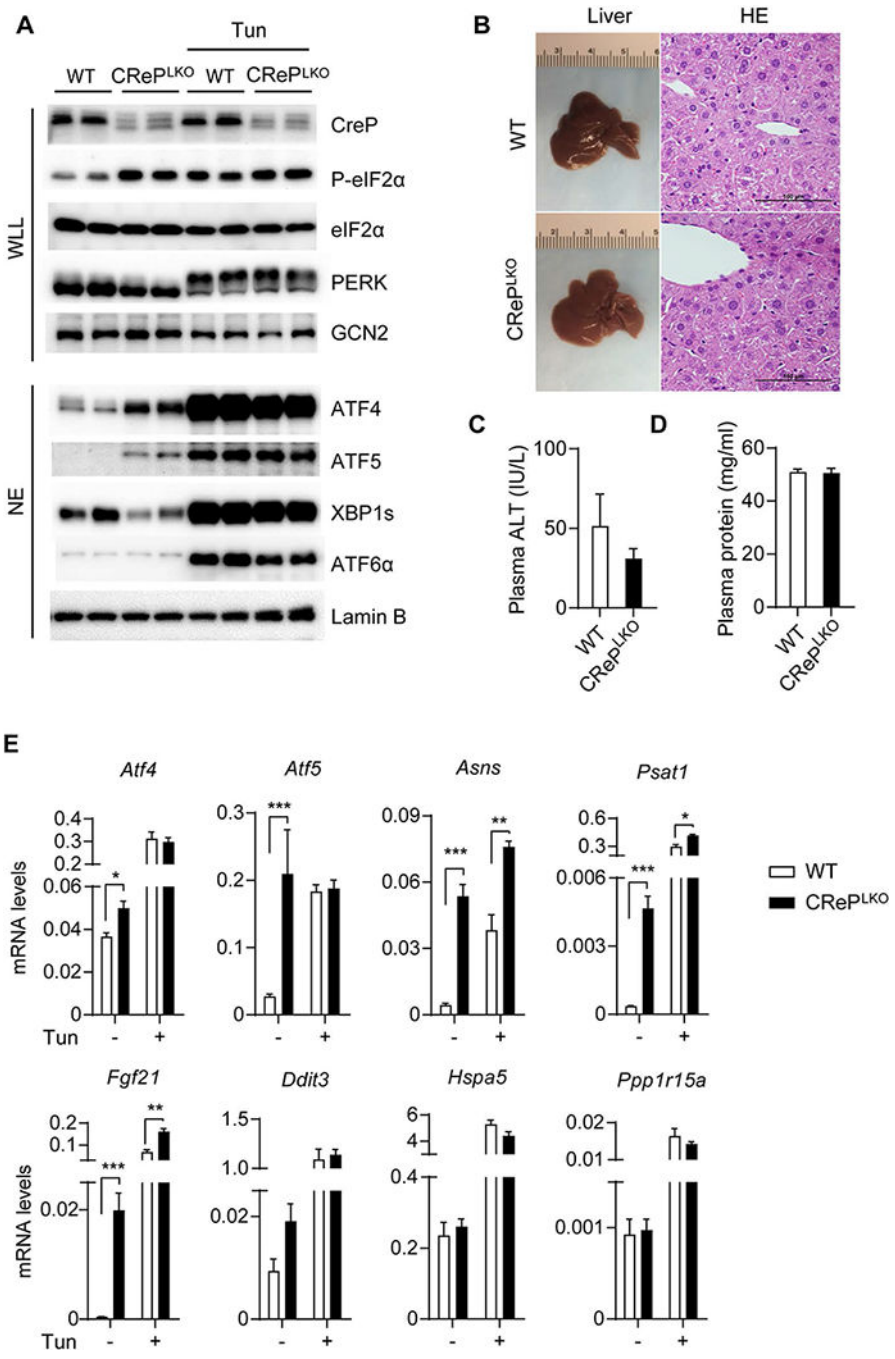

Figure 1. Loss of CReP causes constitutive eIF2α phosphorylation and the downstream ISR activation in the liver. A)

Whole liver lysate (WLL) and nucleus extract (NE) were prepared from the livers of WT and CreP^{LKO} mice, without or with tunicamycin (Tun) injection. Western blots were performed to detect indicated proteins. Phosphorylation of PERK and GCN2 were analyzed by an upward mobility shift on 5% SDS-PAGE gels. **B)** Gross morphology and H&E staining of livers of WT and CreP^{LKO} mice. Scale bars, 100 μm. **C)** Plasma alanine aminotransferase (ALT) levels of WT and CreP^{LKO} mice (n=6). **D)** Plasma total protein levels were

quantitated by Pierce@ bicinchoninic acid (BCA) Protein Assay Kit (n=12). **E)** Hepatic expression of indicated genes were detected by quantitative RT-PCR (n=12, (-) Tun and n=4, (+) Tun). Values were normalized to β-actin. *p<0.05, **p<0.01, ***p<0.001; WT vs CReP^{LKO}. All values are mean ± SEM.

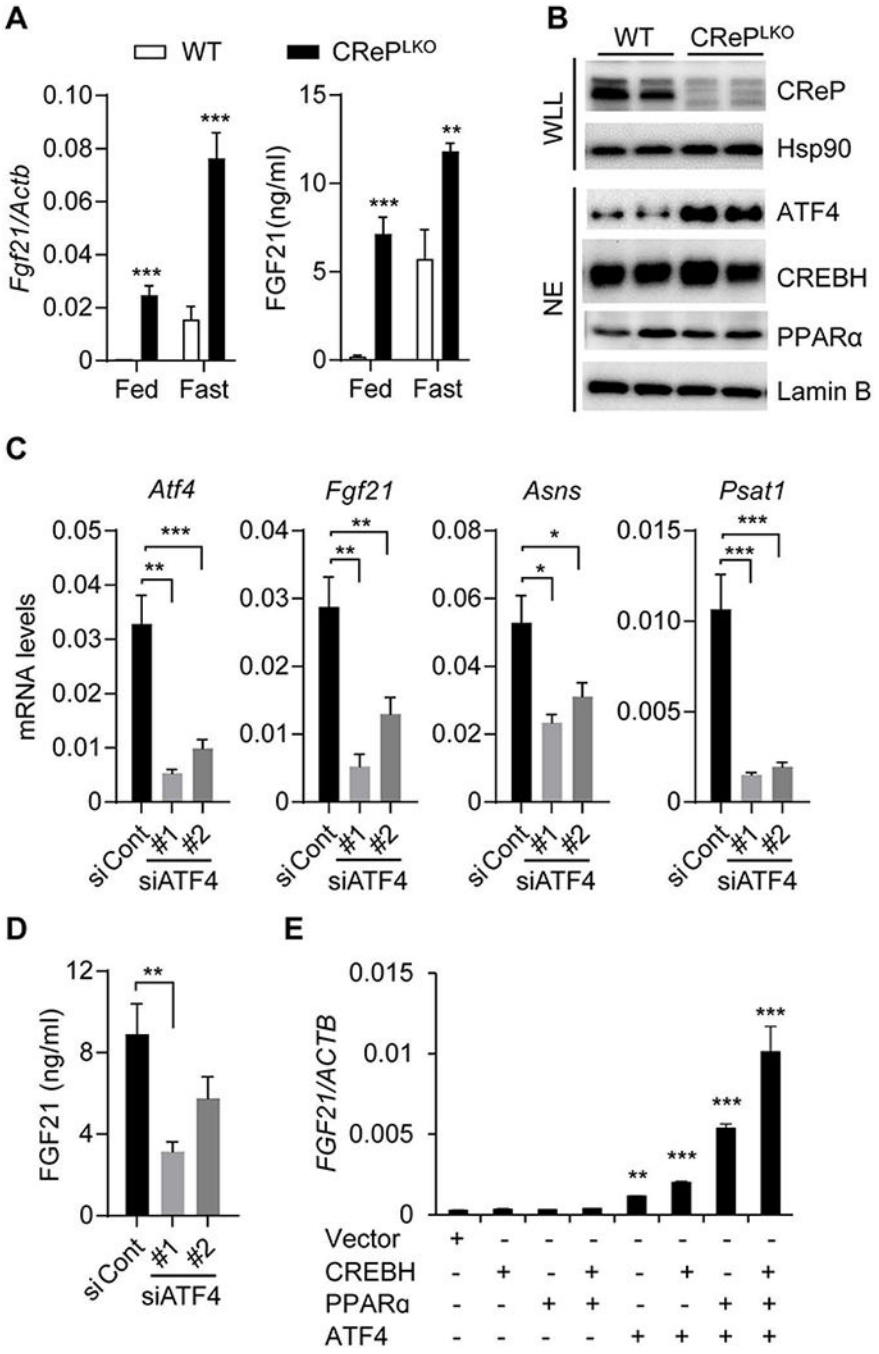

Figure 2. ATF4 is responsible for the constitutive FGF21 production in CReP^{LKO} mice. A) Hepatic Fgf21 mRNA and plasma FGF21 protein levels in WT and CreP^{LKO} mice (n=12) measured in the fed state or after an overnight fasting (16 hours). **B)** Representative western blots to detect CReP in whole liver lysate (WLL) and ATF4, CREBH and PPARα in liver nuclear extracts (NE) (n=6). Hsp90 and Lamin B were used as loading control in WLL and NE fractions, respectively. **C)** Hepatic Atf4, Fgf21, Asns and Psat1 mRNA levels in CreP^{LKO} mice injected with ATF4 siRNA (si #1 and si #2) or a negative control siRNA (si Cont) 3 days before sacrifice. **D)** Plasma FGF21 levels of the indicated siRNA-injected

CreP^{LKO} mice. N=4-8. **E)** *FGF21* mRNA level in HepG2 cells transfected with the indicated combination of plasmids. Values represent mean ± SEM from three independent experiments. *p<0.05, **p<0.01 and ***p<0.001 WT vs CReP^{LKO} or as indicated. All values are mean ± SEM.

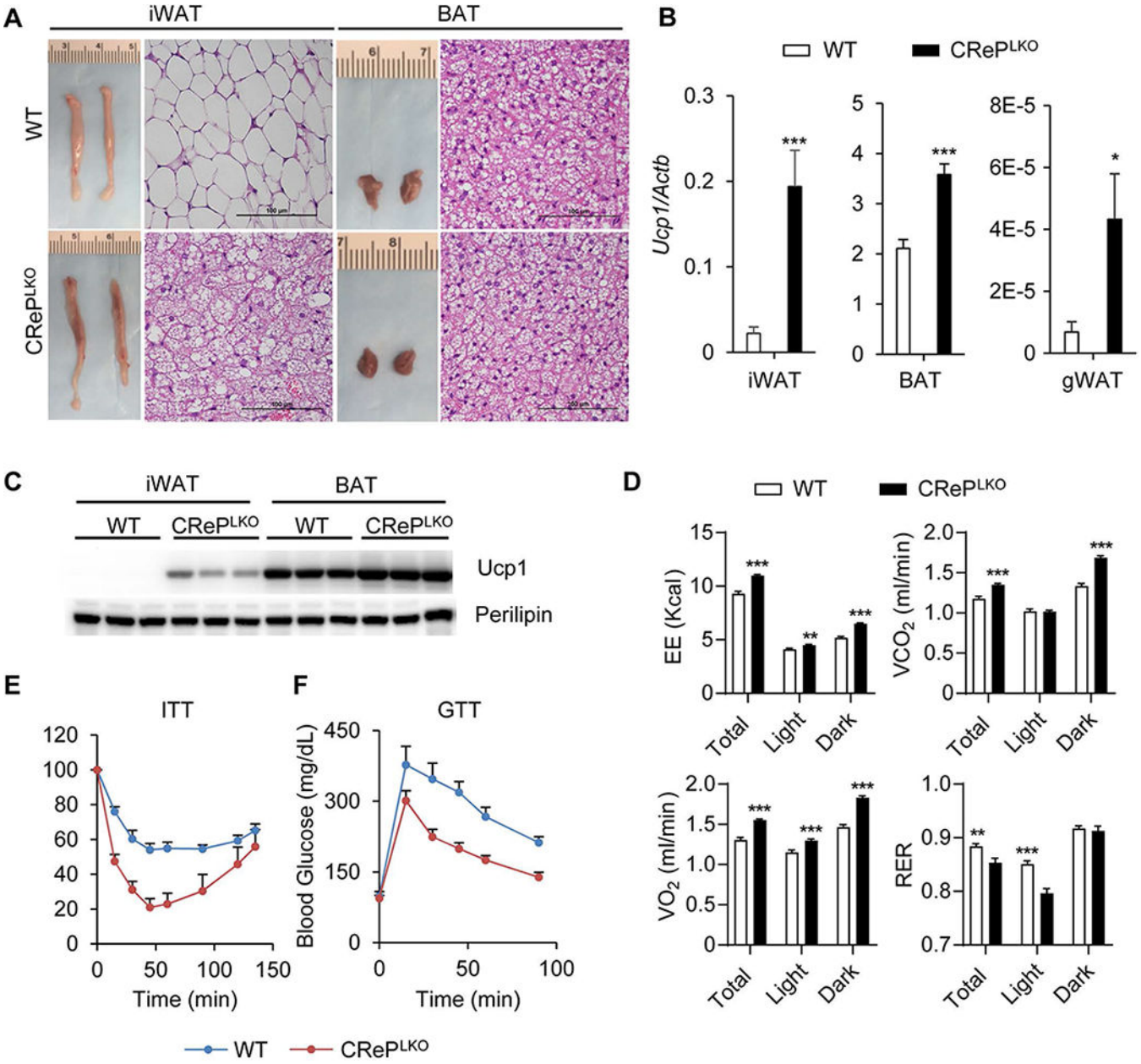

Figure 3. CReP^{LKO} mice exhibit increased beige adipogenesis and improved glucose homeostasis

A) Gross morphology and H&E staining of the inguinal white adipose tissue (iWAT) and brown adipose tissue (BAT) of WT and CreP^{LKO} mice. Scale bars, 100 μm. **B)** Ucp1 mRNA levels in iWAT, BAT and gonadal white adipose tissue (gWAT) determined by qRT-PCR (n=12). **C)** UCP1 western blot of whole tissue lysates. Perilipin was used as a loading control. **D)** Measurement of energy expenditure (EE), O_2 consumption (VO_2) and CO_2 production (VCO_2) in WT and CreP^{LKO} mice on chow diet (n=6).. *p<0.05, **p<0.01 and ***p<0.001; WT vs CReP^{LKO}. **E)** Glucose tolerance test (GTT) and Insulin tolerance test (ITT) of WT and CReP^{LKO} mice (n=6). For ITT, values represent percentage of the beginning blood glucose level. ***p<0.001; WT vs CreP^{LKO} by two-way ANOVA test. All values are mean ± SEM.

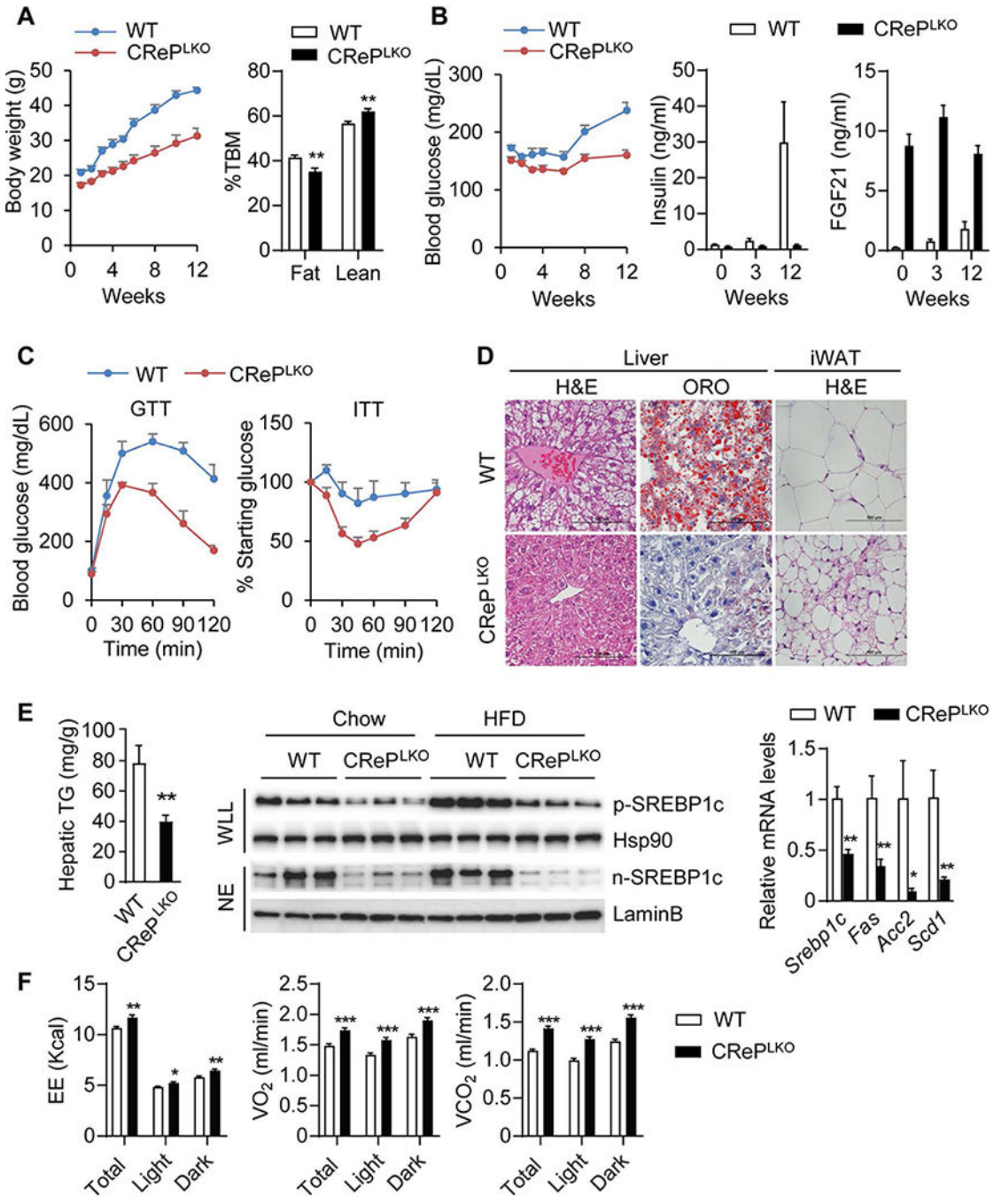

Figure 4. CReP^{LKO} mice are resistant to high fat diet-induced obesity, hepatic steatosis and insulin resistance

A) Body weights and fat and lean mass of WT and CreP^{LKO} mice after 12 weeks of HFD feeding. Fat and lean mass were presented as percentage of total body mass (%TBM). **B)** Blood glucose, plasma insulin and FGF21 levels of WT and CreP^{LKO} mice after HFD feeding. **C)** GTT and ITT of WT and CReP^{LKO} mice after 12-week HFD feeding. N=6-8. ***p<0.001; WT vs CreP^{LKO} by two-way ANOVA. **D)** H&E staining (liver and iWAT) and Oil Red O staining (liver) of WT and CreP^{LKO} mice after 12-week HFD feeding. Scale bars,

100 μm. **E)** Hepatic triglyceride (TG) levels, Srebp1c processing and lipogenic gene expression of WT and $CreP^{LKO}$ mice after 12 weeks of HFD feeding. Srebp1c precursor (p-Srebp1c) and nucleus protein (n-Srebp1c) were blotted in whole liver lysate (WLL) and nucleus extract (NE) from the livers. Hsp90 and LaminB were used as loading controls. Lipogenesis related genes such as Srebp1c, Fas, Scd1 and Acc2 were detected by qPCR. **F)** Measurement of energy expenditure (EE), O_2 consumption (VO_2) and CO_2 production (VCO_2) in WT and $CreP^{LKO}$ mice after 12 weeks of HFD feeding. N=6-8. *p<0.05, **p<0.01 and ***p<0.001; WT vs $CReP^{LKO}$. All values are mean ± SEM.

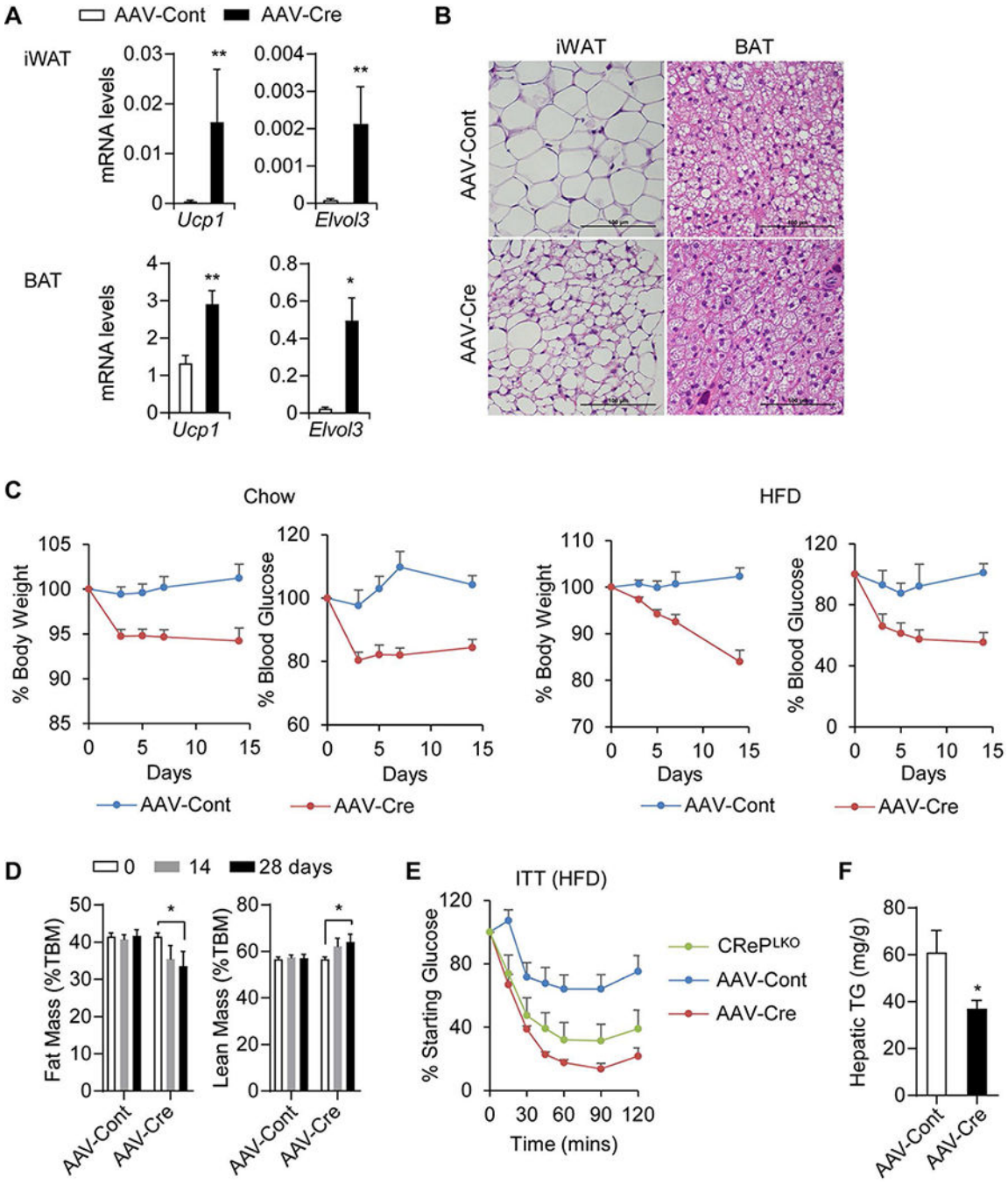

Figure 5. Acute deletion of CReP in the liver induces beige adipogenesis and increased insulin sensitivity. A)

Ucp1 and Elvol3 mRNA leves in the iWAT and BAT of AAV-injected Ppp1r15b^{loxP} mice. N=8-9. *p<0.05 and **p<0.01; AAV-Cont vs AAV-Cre. **B)** H&E staining of iWAT and BAT of the AAV-injected Ppp1r15b^{loxP} mice. Scale bars, 100 μm. **C)** Change of body weight and blood glucose levels of lean and obese Ppp1r15b^{loxP} mice after AAV injection. Ppp1r15b^{loxP} mice were fed with either chow diet or HFD for 3 months prior to AAV injection. The data were presented as the percentage of initial body weight and blood glucose. N=5-6.

***p<0.001; AAV-Cre vs AAV-Cont by two-way ANOVA test. **D)** Fat and lean mass of HFD-fed Ppp1r15b^{loxP} mice before and at 14 and 28 days after injection with AAV-Cre (n=6) or AAV-Cont (n=5). *p<0.05, AAV-Cont vs AAV-Cre as indicated. **E)** ITT performed on HFD-fed Ppp1r15b^{loxP} mice following 7 days of AAV injection. CReP^{LKO} mice was included as a positive control. N=5-6. ***p<0.001; AAV-Cont vs AAV-Cre or CReP^{LKO} by two-way ANOVA test. **F)** Hepatic TG levels of HFD-fed Ppp1r15b^{loxP} mice measured 4 weeks after AAV-injection. N=8-9, *p<0.05; AAV-Cont vs AAV-Cre. All values are mean ± SEM.

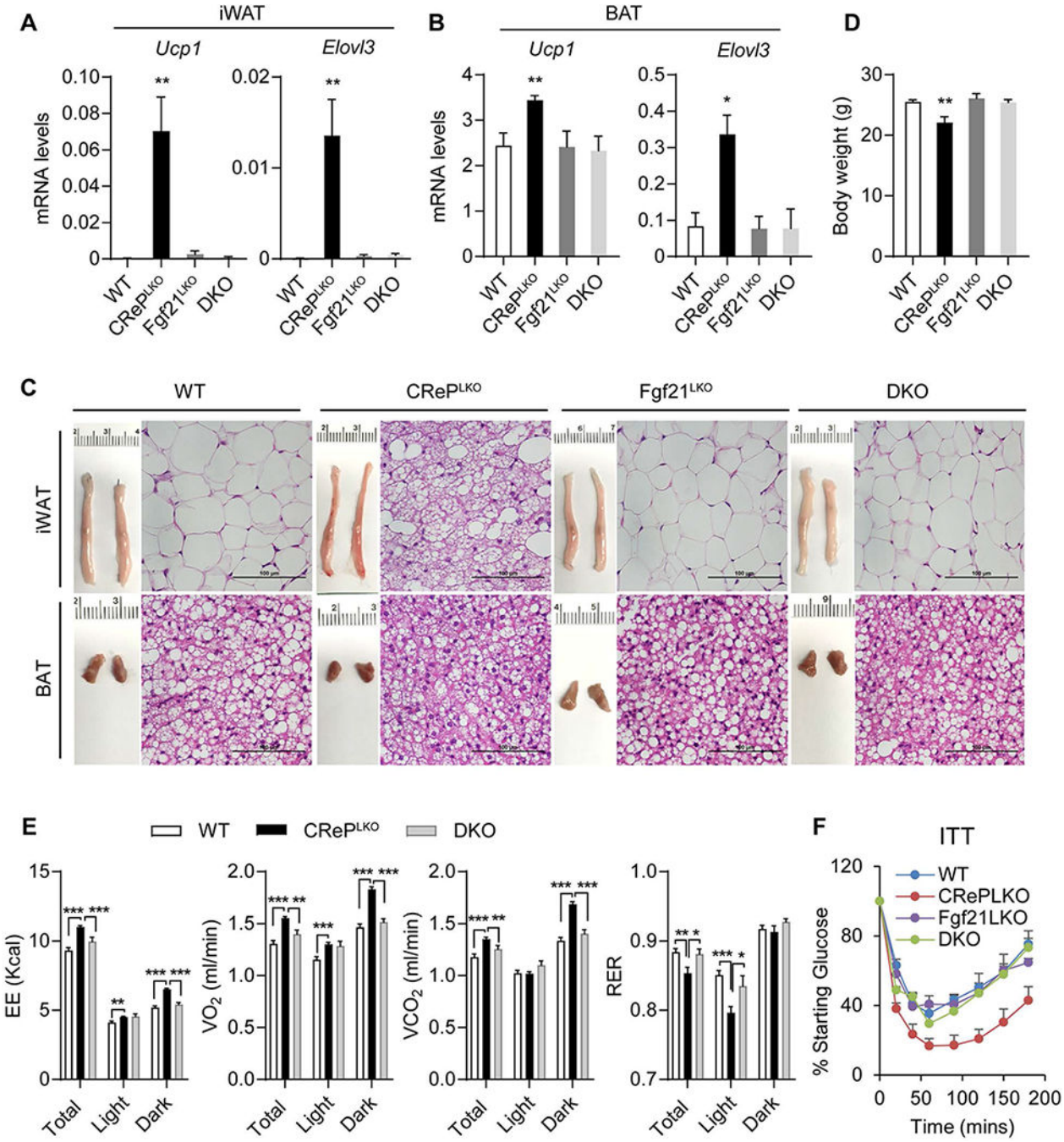

Figure 6. FGF21 is critical for the improved metabolic parameters of CReP^{LKO} mice. A) Ucp1 and Elvol3 mRNA levels in iWAT and **B)** BAT of WT (n=7), CReP^{LKO} (n=7), Fgf21^{LKO} (n=5) and DKO mice (n=6). **C)** H&E staining of iWAT and BAT of WT, CReP^{LKO}, Fgf21^{LKO} and DKO mice. Representative images from 6 mice per group are shown. Scale bars, 100 μm. **D)** Body weights of WT (n=25), CReP^{LKO} (n=7), Fgf21^{LKO} (n=5) and DKO (n=10) mice. *p<0.05, **p<0.01; CReP^{LKO} vs WT, Fgf21^{LKO} or DKO. **E)** Measurement of energy expenditure (EE), O_2 consumption (VO_2) and CO_2 production (VCO_2) in WT, CreP^{LKO} and DKO mice (n=8 per group) after 12 weeks of HFD feeding.

*p<0.05, **p<0.01 and ***p<0.001 as indicated between CReP^{LKO}, WT or DKO. **F)** ITT of WT (n=8), CReP^{LKO} (n=6), Fgf21^{LKO} (n=5) and DKO (n=6) mice. ***p<0.001; CReP^{LKO} vs WT, Fgf21^{LKO} or DKO by two-way ANOVA test. All values are mean ± SEM.

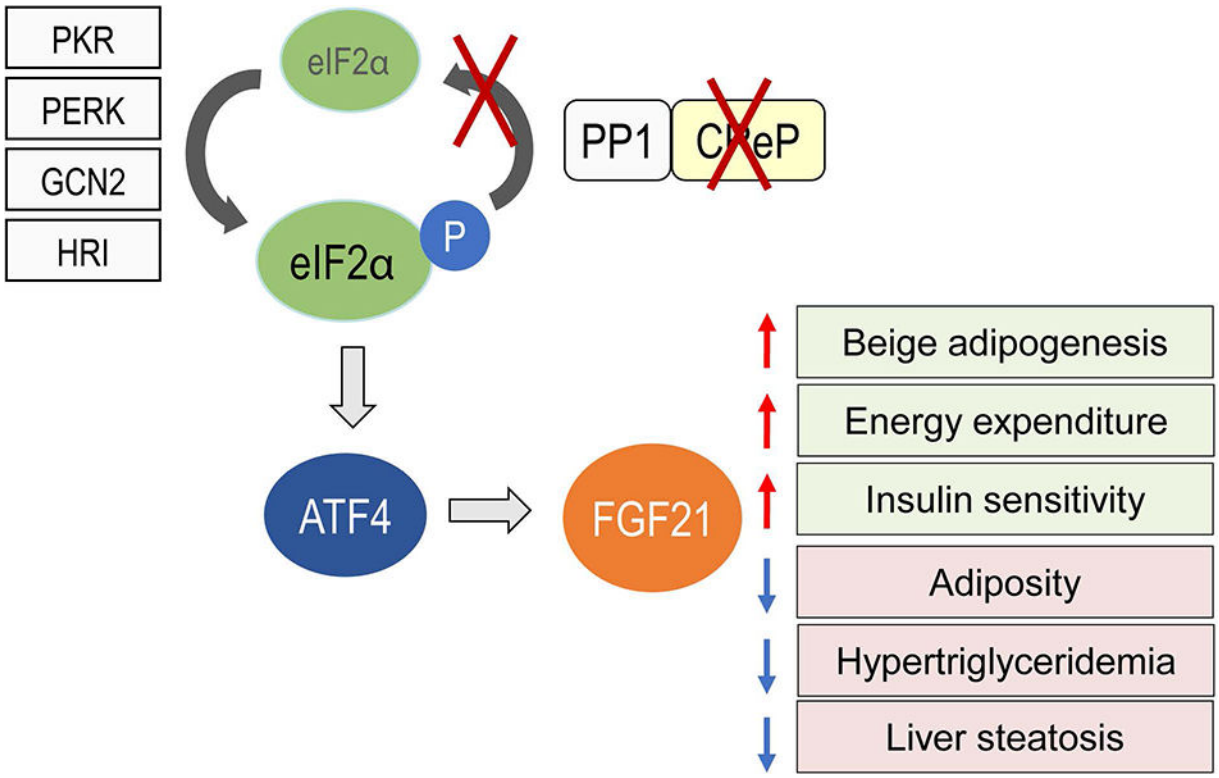

Figure 7. Loss of CReP in the liver causes ISR activation and improves metabolic health

CReP deletion causes constitutive eIF2α phosphorylation in the liver, which leads to activation of ATF4 transcriptional program including increased FGF21 production. FGF21 production in the liver of $CReP^{LKO}$ mice promotes multiple beneficial effects on metabolism, including increased beige adipogenesis, energy expenditure and insulin sensitivity, and decreased adiposity, plasma lipids and liver steatosis.